Cryogenics 116 (2021) 103295

Contents lists available at ScienceDirect

Cryogenics

journal homepage: www.elsevier.com/locate/cryogenics

Research paper

Investigation of microhardness properties of the multi-walled carbon nanotube additive MgB_2 structure by using the vickers method

Naki Kaya [a,*], Şükrü Çavdar [b], Özgür Öztürk [c], Hakan Ada [d], Haluk Koralay [b]

[a] Opticianry Program, Vocational School, T.C. İstanbul Arel University, 34295 İstanbul, Turkey
[b] Superconductivity and Thermal Analysis Laboratory (STAL), Department of Physics, Faculty of Science, Gazi University, 06531 Ankara, Turkey
[c] Faculty of Engineering and Architecture, Department of Electrical and Electronics Engineering, Kastamonu University, 37100 Kastamonu, Turkey
[d] Faculty of Engineering and Architecture, Department of Mechanical Engineering, Kastamonu University, 37100 Kastamonu, Turkey

ARTICLE INFO

Keywords:
Superconductivity
MgB_2
Multi-Walled Carbon Nanotube
Vickers Microhardness

ABSTRACT

In this study, the effect of multi-walled carbon nanotube doping to MgB_2 compound on microhardness properties of MgB_2 was investigated by using solid-state reaction method. The amount of multi-walled carbon nanotubes was chosen as 0, 1, 2, 3 and 4% by weight of total MgB_2. All samples were obtained by sintered at 650 °C temperatures. The microhardness properties of the samples obtained were examined using the Vickers method. At the same time, the samples obtained were analyzed according to Meyer's Law, proportional sample resistance (PSR) model, Hays-Kendall (HK) approach and elastic/plastic deformation (EPD) model. Samples were found to exhibit indentation size effect (ISE) behavior. It was understood that the multi-walled carbon nanotubes doped to the samples made MgB_2 softer by reducing the intergranular bonding of the MgB_2 structure. In addition, it was found that the force applied to the samples caused both plastic and elastic deformation on the samples.

1. Introduction

Although the MgB_2 compound has been known since the early 1950s [1] Akimitsu et al. discovered in 2001 that this compound is a superconductor [2]. After this discovery, studies on MgB_2 continue without slowing down. MgB_2 is a widely used compound in superconductor technology due to the advantages of MgB_2 such as its simple crystal structure [3] high critical transition temperature in metals and alloys, long coherence length and strong intergranular bonds, high critical current density, low anisotropy, optimal intergranular boundaries for high current transport, and low cost [4].

Carbon nanotubes discovered by Sumio Iijima in 1991 have positive properties such as structural, mechanical, electrical and thermal conductivity [5]. Because of such properties, carbon nanotubes are highly preferred in nano-technological studies. After the positive effects of carbon and carbon nanotubes on MgB_2 were discovered, many researchers made the doping of carbon or carbon nanotubes to the MgB_2 superconductor with different methods and in different amounts [6–17].

The microhardness properties of the samples obtained in this study were examined by the Vickers method. At the same time, the samples were analyzed according to Meyer's Law, proportional sample resistance (PSR) model, Hays-Kendall (HK) approach and elastic/plastic deformation (EPD) model.

Many studies showed that the microhardness properties of the materials depend on the load applied to the material [18–24]. With the Vickers method, some values such as surface tension of samples, microhardness values independent of load, elastic modulus can be reached in the analysis of samples.

Eqs. (1)–(4) is used in Vickers analysis.

$$H_V = 1854.4 \times \frac{F}{d^2} \tag{1}$$

$$d = \frac{d_1 + d_2}{2} \tag{2}$$

$$E = 81.9635 \times H_V \tag{3}$$

$$Y \cong \frac{H_V}{3} \tag{4}$$

Here, H_V is the Vickers hardness value, d_1 and d_2 are the diagonal length of the indentation trace formed on the sample, E is the elastic modulus and Y is the stress value.

In the literature, when interpreting the microhardness values of materials, 2 different types of behavior are mentioned. The first of these is a behavior called indentation size effect (ISE), which is expressed as

* Corresponding author.

https://doi.org/10.1016/j.cryogenics.2021.103295
Received 15 October 2020; Received in revised form 19 March 2021; Accepted 28 March 2021
Available online 31 March 2021

the microhardness value decreases with the load applied to the material surface. Both elastic deformation and plastic deformation are seen in such materials. Another is the reverse indentation size effect (RISE). In this case, it shows an increasing microhardness value against the load applied to the material. In addition, these materials only exhibit plastic deformation. Elastic deformation is not observed or it is very small compared to plastic deformation.

It is very important to support the experimental tests performed to characterize the mechanical properties with theoretical modeling. In this context, the models in the literature and explained below (Meyer's law, PSR model, HK approach and EPD model) were applied to our experimental data. The main purpose here is to calculate load-dependent microhardness values as well as load-independent microhardness values.

Theoretical models applied to experimental data are explained as follows.

Meyer's Law is the simplest and most fundamental law used to explain the behavior of ISE. According to this law, there is a relationship below between the indentation load (F) and the average of the diagonal lengths (d) (Eq. (5)).

$$F = Ad^n \tag{5}$$

Here, the value of n is the Meyer exponent, which is a measure of ISE-RISE behavior. If the Meyer exponent is less than 2 ($n < 2$) it confirms that the displacement character is ISE, and if it is greater than 2 ($n > 2$) the displacement character is RISE. The fact that n value is 2 ($n = 2$) gives the case of hardness independent of the load and ISE behavior is not observed in the material [25,26].

In addition, the Meyer index value also gives information about whether the material is hard or soft. A case of $1 < n < 1.6$ means that the material is a hard material, and $1.6 < n$ means that the material is soft [25].

PSR model: In the PSR model used to analyze the ISE behavior, it is stated that the sample resistance is not constant and increases with the depth of indentation. Eq. (6) expressing this model is given below.

$$F = W_{PSR}d + A_{PSR}d^2 \tag{6}$$

In the equation, W_{PSR} and A_{PSR} are constants for elastic deformation and plastic deformation, respectively, and are determined from the slope of the (F/d)-d graph and the point where it intersects the y-axis, respectively. A_{PSR} is used in real microhardness value calculations. In this approach, the microhardness value independent of the load is calculated by Eq. (7).

$$H_{PSR} = 1854.4 \times A_{PSR} \tag{7}$$

Hays ve Kendall (HK) approach is a hardness model that states that a minimum load value (W) must be present in order to create permanent deformation in the sample. They argued that if the applied load cannot exceed this resistance, permanent deformation will not occur and only elastic deformation will occur. In other words, if a test load is below a certain limit value, only elastic deformation can be created, and if it is above this value, both plastic and elastic deformation can be created. Eqs. (8)–(9) is used for the HK approach.

$$F_{etkin} = F - W_{HK} \tag{8}$$

$$F - W_{HK} = A_{1HK}d^2 \tag{9}$$

In this approach, the microhardness value independent of the load can be found by Eq. (10).

$$H_{HK} = 1854.4 \times A_{HK} \tag{10}$$

Here, A_{HK} is a constant independent of applied load, and W is the minimum amount of load required to create a trace. W and A_{HK} values are calculated from $F - d^2$ graph and the slope obtained from this graph will give us the value of $A_{HK} \times A$ positive W_{HK} value is interpreted as the applied load is sufficient to create both plastic deformation and elastic deformation on the sample [27].

On the basis of **the EPD model**, there is a relationship between the size of the indentation and the applied load [28–29]. In most indentation tests, the indentation size is measured after the indentation is removed from the sample. Elastic recovery occurs around the remaining indentation trace after the tip is removed. Thus, the indentation size shrinks to a certain extent. Considering this, it is deemed appropriate to add a new term to the measured indentation size to calculate the hardness value independent of the load (Eq. (11)).

$$F = A(d_p + d_e)^2 \tag{11}$$

Here d_e is related to elastic deformation and d_p is related to plastic deformation. A is a constant of the sample. A and d_e values are calculated from the graph of $F^{1/2} - d_p$. Also, the microhardness value independent of the load is defined by Eq. (12).

$$H_{EPD} = 1854.4 \times A \tag{12}$$

2. Methods

2.1. Experimental details

Magnesium (Mg) powder (>99% purity, Sigma-Aldrich), amorphous nano Boron (B) powder (≥95% purity, Sigma Aldrich) and multi-walled carbon nanotube powders (≥90% purity, Sigma Aldrich) were used. MgB_2 samples without additives and with 1, 2, 3, 4% by weight multi-walled carbon nanotubes doped were produced by solid-state reaction method. The samples obtained were named with 5 different codes. The name of 0 sample was given for the MgB_2 produced without any additives, while the samples doped with multi-walled carbon nanotubes in the ratio of 1, 2, 3 and 4% were named as 1, 2, 3 and 4 samples, respectively. The 0 sample was produced without any additives. Multi-walled carbon nanotubes were added to 1 sample as 1% of the total weight of the sample, 2 samples as 2% of the total weight of the sample, 3 samples as 3% of the total weight of the sample and 4% of the total weight of the sample. Magnesium and boron powders were mixed with Retsch PM 400 brand automatic mixer device for 3 h, and then multi-walled carbon nanotube powders were added to the resulting MgB_2 mixture and mixed manually in agate mortar for half an hour. Each powder mixture was pressed under a pressure of 2 tons cm^{-2} and sintered at 650 °C for 1 h in an argon atmosphere. Microhardness measurements of the obtained samples were made with Shimadzu HVM-2 model digital microhardness measuring device, X-ray diffraction (XRD) analysis was performed with Rigaku Mini Flex 2 brand x-ray diffraction meter device and scanning electron microscopy (SEM) analyses were performed with Jeol-JSM 6060 LV brand scanning electron microscope.

3. Results and discussions

3.1. XRD analysis results

XRD measurements were made with Rigaku Mini Flex 2 X-ray powder diffractometer using Cu-K_α beam in the $20^0 \leq 2\theta \leq 80^0$ range.

In Fig. 1, characteristic plane peaks of (0 0 1), (1 0 1), (0 0 2), (1 0 2), (2 0 0) and (2 0 1) of MgB_2 were seen in all samples. It was observed that the peak of the (1 0 1) plane is more severe than the peak of the other planes. The width of the plane peak (1 0 1) of sample no. 2 is narrower and more severe than the other samples. Narrow peak width and increase in peak intensities in X-ray diffraction patterns indicate a smoother crystographic transition, that is, a better crystallinity [30]. Therefore, the crystographic structure of the sample number 2 is smoother than the other samples. In the samples obtained, some expansion is observed in all plane peaks due to doping. This occurs when

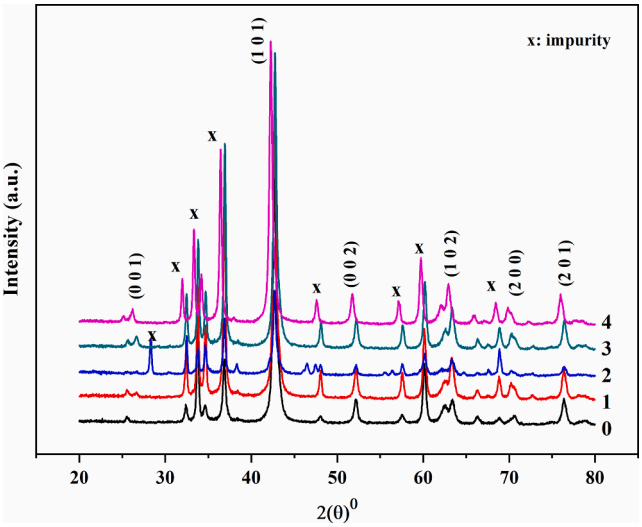

Fig. 1. XRD patterns of the samples obtained.

multi-walled carbon nanotube atoms, which are included in the structure as a result of multi-walled carbon nanotube doping, enter between Mg and B atoms. In this case, it is thought that the bond between the Mg and B atoms is subjected to some stress, so the lattice parameters are damaged and the crystal structure is damaged. Crystal size calculation is made with Scherrer Equation shown by Eq. (13) [31].

$$D = \frac{K \cdot \lambda}{\beta . cos\theta} \tag{13}$$

Here, D represents the particle size, λ shows the wavelength of the X-ray, β indicates half the width of the highest intensity peak and θ represents the angle of this peak. The multi-walled carbon nanotube additive had a reducing effect on the particle size. In some studies with different additives, it was observed that increasing the doping rate decreases particle size and intergranular pores [32,33]. Table 1 was created according to the calculated particle size results. As can be understood from Table 1, it was observed that the particle size of the doping (with sample 0) slightly reduced compared to the sample without doping. In addition, when we compared the samples with additives among themselves, it was seen that there was a partial increase with additive.

For the hexagonal structure shown by Eq. (14), the lattice parameters of the MgB_2 samples were found by using the lattice parameter calculation equation.

$$\frac{1}{d^2} = \frac{4}{3}\left[\frac{h^2 + hk + k^2}{a^2}\right] + \frac{l^2}{c^2} \tag{14}$$

In this equation d are the interplanar distance, h, k, l are Miller indices, a and c are the lattice parameters. Since $a = b$ in the hexagonal structure, the value a is also defined as the value b. Table 2 was created for the lattice parameters found as a result of the calculations. When Table 2 is examined, it is clearly seen that the lattice parameters a, b and c of all samples are almost the same. This means that there is no change in the crystal structure with the doping. This is the reason why we see the same diffraction peaks at the same angles from the XRD graph. The lattice parameters obtained as a result of the calculation also support our XRD data.

Table 1
Granular sizes of the samples obtained.

	Sample 0	Sample 1	Sample 2	Sample 3	Sample 4
Granular size (nm)	21.50	19.68	20.03	19.83	21.37

Table 2
Lattice parameters of the samples obtained.

Lattice Parameters	Sample 0	Sample 1	Sample 2	Sample 3	Sample 4
a = b (nm)	0.284	0.280	0.281	0.283	0.284
c (nm)	0.426	0.421	0.422	0.425	0.426

3.2. SEM analysis results

Fig. 2: In a, b, c, d, e, there are SEM images at equal magnification of the multi-walled carbon nanotube doped samples at 0, 1, 2, 3 and 4% respectively. The filamentous structures in the images are multi-walled carbon nanotubes. In all of the images, it is understood that multi-walled carbon nanotubes maintain their traditional appearance and do not undergo deformation. When Fig. 2 a is examined, it is seen that the structure is generally found in large pieces due to pressing. It can be said that this increases the intergranular connection. In Fig. 2 b, c, d, e, the MgB_2 structures are separated from each other. The separation of MgB_2 in small pieces increased with the increase in the rate of contribution. This is a result of multi-walled carbon nanotubes preventing large clusters. The fact that the structure is not in bulk directly affects the microhardness properties. In Fig. 2 c, it is seen that multi-walled carbon nanotubes do not accumulate on the surface; on the contrary, they penetrate more into the structure. This situation has increased with the increase in the rate of contribution.

3.3. Microhardness measurement results

3.3.1. Analysis results according to the Vickers method

In this study, microhardness values are measured using a Vickers microhardness tester for its common usage and non-destructive measuring conditions regarding to the sample surfaces. Force is applied from 25 N to 300 N on the material's surface, and diagonals of the trace left by the indenter are read using the microscope and load/trace area. Vickers hardness is calculated using the relation given in Eq. (1). It can be seen from Fig. 3 that the microhardness values decrease with increasing the doping level and applied load. This is known as ISE behavior [34] and according to the results obtained, samples were found to have ISE behavior. Microhardness values have reached the plateau (saturation region) around about 2 N for the samples. Parameters such as modulus of elasticity (E) and yield strength (Y) that are as important as hardness to mechanical characterizations of materials are also calculated and values of these parameters are given in Table 3.

In a study in which Bulk MgB_2 sample was examined, it was determined that MgB_2 showed ISE behavior [35]. This result is consistent with Table 3 and Fig. 3. Studies show that all samples examined in terms of microhardness properties must reach a limit plateau value where the microhardness values do not change too much against a certain external load applied [36–37]. It is seen that the samples entered the plateau region at values above 2 N of the applied load. When the samples are compared with each other, it is seen that the multi-walled carbon nanotube additive applied to the sample and the annealing process applied to take place of the reaction creates a softness-increasing effect on the sample and decreases the surface tension in the sample. This is the result of the multi-walled carbon nanotubes entering between the Mg and B atoms during the chemical reaction, causing the intergranular connection between Mg and B to decrease. The observation of small clusters in the doped samples in SEM images explains this situation.

3.3.2. Microhardness analysis result according to Meyer's Law

The graph shown in Fig. 4 was drawn by calculating the InF and Ind values stipulated by Meyer's Law. For each sample, Meyer exponent (n), InA_{1k} and H_V values were found and Table 4 was created. It is seen in Table 4 that the Meyer exponent value is greater than 1.6. Therefore, it is concluded that the materials are soft [26].

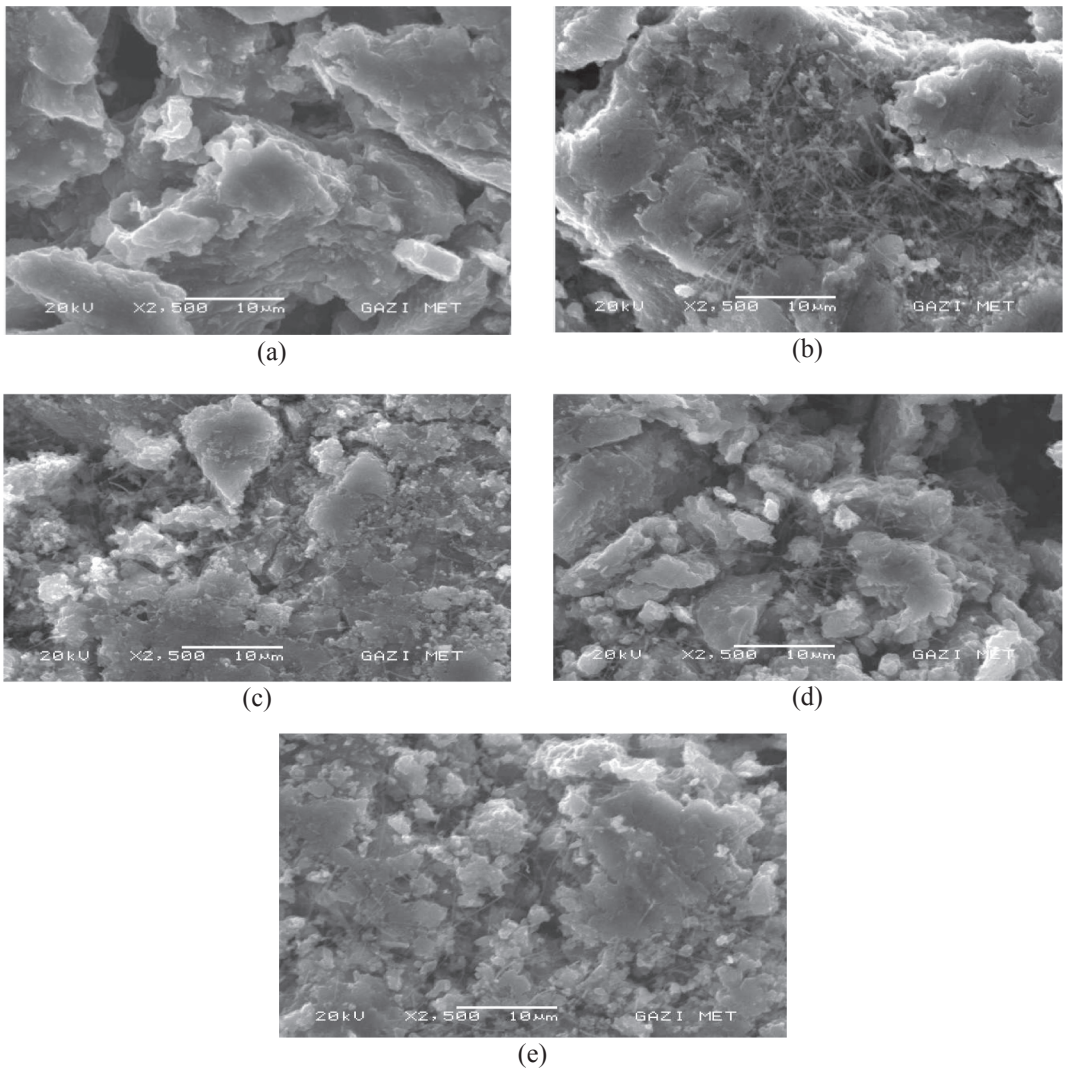

Fig. 2. SEM images of (a) Sample 0, (b) Sample 1, (c) Sample 2, (d) Sample 3, and (e) Sample 4.

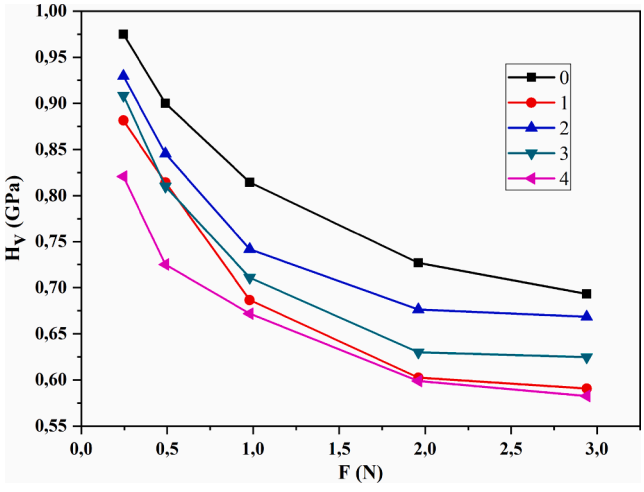

Fig. 3. Graph of change of microhardness values of samples with applied load according to Vickers method.

The slope of the graph gives the value of n, and the point where it intersects the vertical axis gives the value of A_K. If the Meyer exponent value is less than 2 for the samples examined, it confirms that the load-

Table 3
Microhardness values calculated for samples according to the Vickers method.

Sample	F (N)	Hv (GPa)	Y	E(Gpa)
0	0.24	0.97	0.32	79.90
	0.49	0.90	0.30	73.76
	0.98	0.81	0.27	66.75
	1.96	0.72	0.24	59.58
	2.94	0.69	0.23	56,82
1	0.24	0.88	0.29	72.25
	0.49	0.81	0.27	66.75
	0.98	0.68	0.22	56.27
	1.96	0.60	0.20	49.39
	2.94	0.59	0.19	48.41
2	0.24	0.93	0.30	76.18
	0.49	0.84	0.28	69.30
	0.98	0.74	0.24	60.79
	1.96	0.67	0.22	55.44
	2.94	0.66	0.22	54.77
3	0.24	0.90	0.30	74.47
	0.49	0.81	0.26	66.38
	0.98	0.71	0.23	58.25
	1.96	0.63	0.21	51.64
	2.94	0.62	0.20	51.19
4	0.24	0.82	0.27	67.27
	0.49	0.72	0.24	59.44
	0.98	0.67	0.22	55.06
	1.96	0.59	0.19	49.08
	2.94	0.58	0.19	47.75

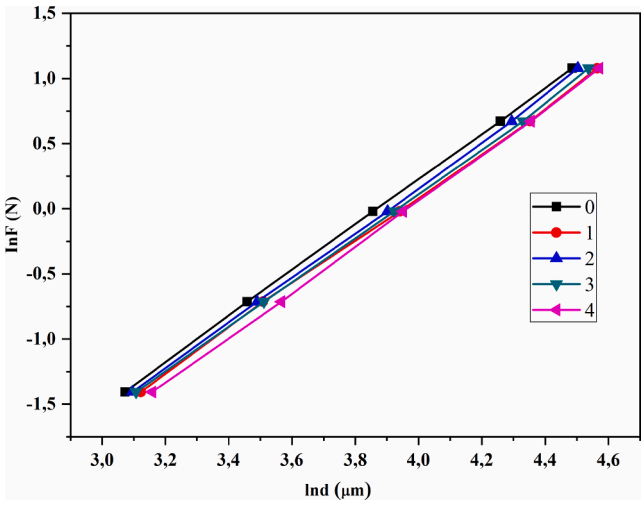

Fig. 4. InF- lnd graph of samples according to Meyer's Law.

Table 4
Parameters obtained with experimental data according to Meyer's Law.

Samples	n	InA_{1k} (GPa)	H_v (GPa)
0	1.75	−6.78	0.97–0.69
1	1.70	−6.70	0.88–0.59
2	1.75	−6.83	0.92–0.66
3	1.72	−6.77	0.90–0.62
4	1.75	−6.96	0.82–0.58

dependent displacement character is in the form of ISE behavior. These data are summarized in Table 4.

3.3.3. Microhardness analysis result according to PSR model

The F/d-d graph shown in Fig. 5 was drawn by using the basic data obtained as a result of the Vickers analysis and the data obtained were summarized in Table 5.

A negative or positive W_{PSR} value indicates the ISE or RISE behavior of the samples obtained. Such that if W_{PSR} is negative, samples show RISE behavior, and if W_{PSR} is positive, samples show ISE behavior. As seen in Table 5, the W_{PSR} value was positive in all samples. So, all samples are ISE behavior. As can be seen, the α values of the samples showing ISE behavior are positive. This indicates that there is both elastic deformation and plastic deformation in all samples. In addition, the transition values of the samples to the plateau are far from the load-independent hardness values calculated with the PSR model. This shows

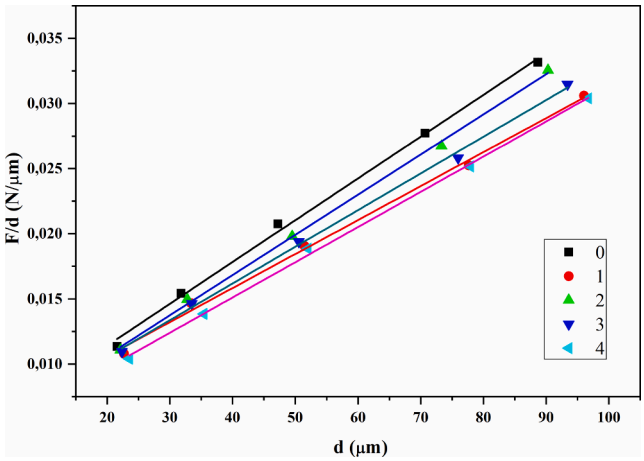

Fig. 5. F/d-d graph of the samples according to the PSR model.

Table 5
Parameters obtained with experimental data according to the PSR model.

Samples	A (N μm^{-1})	B (N μm^{-2})	W_{PSR} (N μm^{-1})	H_{PSR} (GPa)	Hv (GPa)
0	3.09×10^{-4}	500×10^{-5}	49×10^{-4}	59×10^{-2}	0.97–0.69
1	2.61×10^{-4}	539×10^{-5}	53×10^{-4}	48×10^{-2}	0.88–0.59
2	3.08×10^{-4}	449×10^{-5}	44×10^{-4}	55×10^{-2}	0.92–0.66
3	2.81×10^{-4}	491×10^{-5}	49×10^{-4}	51×10^{-2}	0.90–0.62
4	2.70×10^{-4}	429×10^{-5}	42×10^{-4}	50×10^{-2}	0.82–0.58

that this model is insufficient in determining the real hardness values of the samples obtained by this study.

3.3.4. Microhardness analysis result according to EPD model

Fig. 6 and Table 6 were created with the calculations predicted by the EPD model.

In the EPD model, a negative or positive value gives information about whether elastic or plastic deformation has occurred on the sample. If the d_e value is negative, it indicates that no elastic deformation occurs on the sample with the load applied to the sample, but plastic deformation occurs, while if the $d_e$value is positive, it indicates that both plastic and elastic deformation occurs.

As seen in Table 6, the d_e value found from the slope of the graph was positive for all samples showing ISE behavior. In other words, not only plastic deformation but also elastic deformation was not observed in the applied loads. Hardness values calculated with the EPD model are also quite far from the plateau region. As a result, it is clearly seen that the EPD model is insufficient in determining the actual hardness values for all samples obtained.

3.3.5. Microhardness analysis result according to HK approach

Fig. 7 and Table 7 were created according to the HK approach. While microhardness measurement is made by applying an external force to a sample, according to the HK approach, it is understood from the negative W_{HK} value that sufficient force has been reached for plastic deformation but not suitable force is created for elastic deformation. If this value is positive, it is concluded that both elastic and plastic deformation occurs.

In Table 7, load-independent hardness value W_{HK} and A_{HK} values are given. Here, the positive W_{HK} value of the samples displaying ISE behavior can be interpreted as the applied load is sufficient to create

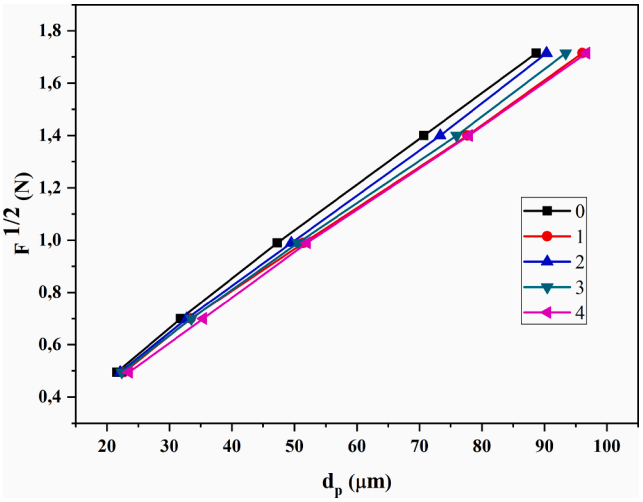

Fig. 6. $F^{1/2}$-d_p graph of samples according to EPD model.

Table 6
Parameters obtained with experimental data according to the EPD model.

Samples	d_e (μm)	H_{EPD} (GPa)	H_v (GPa)
0	11×10^{-2}	16×10^{-1}	0.97–0.69
1	13×10^{-2}	14×10^{-1}	0.88–0.59
2	11×10^{-2}	16×10^{-1}	0.92–0.66
3	12×10^{-2}	15×10^{-1}	0.90–0.62
4	11×10^{-2}	14×10^{-1}	0.82–0.58

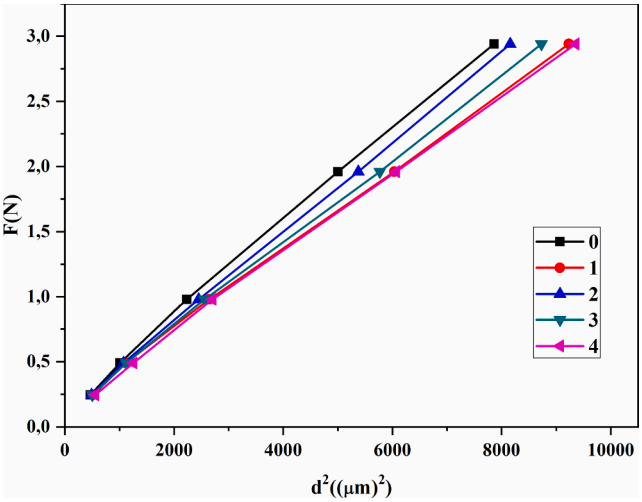

Fig. 7. F-d^2 graph of samples according to HK approach.

Table 7
Parameters obtained with experimental data according to the HK approach.

Samples	A_{1HK}	W_{HK} (N)	H_{HK} (GPa)	Hv (GPA)
0	36×10^{-5}	12×10^{-2}	66×10^{-2}	0.97–0.69
1	30×10^{-5}	13×10^{-2}	55×10^{-2}	0.88–0.59
2	34×10^{-5}	10×10^{-2}	63×10^{-2}	0.92–0.66
3	32×10^{-5}	11×10^{-2}	59×10^{-2}	0.90–0.62
4	30×10^{-5}	11×10^{-2}	55×10^{-2}	0.82–0.58

both plastic deformation and elastic deformation.

The hardness values calculated with the HK approach are very close to the plateau region. For this reason, it is seen that HK approach is much more adequate than other models in determining the real hardness values. The hardness values in the plateau region were reached with the HK approach among the models applied so far for the samples showing ISE behavior. For this reason, we can say that HK approach is the most successful model in theoretically characterizing the mechanical properties of materials.

4. Conclusions

In this study, the effect of microhardness properties of multi-walled carbon nanotube doping to MgB_2 compound was investigated by using solid-state reaction method. It was observed that the inclusion of multi-walled carbon nanotubes in the structure increased the softness and penetration depth of the samples, and also reduced the surface tension of the samples. Both plastic and elastic deformation occurred as a result of external force applied to the samples. It was seen that all of the samples had ISE behavior in terms of microhardness character. In addition, with the multi-walled carbon nanotube doping, decreases in lattice parameters and crystal sizes of all samples were observed compared to the sample without additive. It was seen that the most successful model in explaining the microhardness behavior of the samples was the HK approach.

Declaration of Competing Interest

The authors declare that they have no known competing financial interests or personal relationships that could have appeared to influence the work reported in this paper.

Acknowledgements

We would like to express our gratitude to the Kastamonu University Central Research Laboratory and Gazi University Thermal Analysis Laboratory who contributed to this study.

References

[1] Buzea C, Yamashita T. Review of superconducting properties of MgB_2. Supercond Sci Technol 2001;14(11). https://doi.org/10.1088/0953-2048/14/11/201.
[2] Nagamatsu J, Nakagawa N, Muranaka T, Zenitani Y, Akimitsu J. Superconductivity at 39 K in magnesium diboride. Nature 2001;410(6824):63–4. https://doi.org/10.1038/35065039.
[3] Maki K, Posazhennikova AI, Dahm T. Anisotropic upper critical field in single crystal MgB_2. J Low Temp Phys 2003;131(5):1199–204. https://doi.org/10.1023/A:1023486001526.
[4] Safran S. Karbon kaplı nano-bor kullanılarak hazırlanan süperiletken MgB2 numunelerde magnezyum kaynağının yapısal ve elektriksel özellikler üzerindeki rolü. Gazi Uni J. Sci Part C 2018;6(3):715–20.
[5] Lijima S. Helical microtubules of graphitic carbon. Nature 1991;354:56–8. https://doi.org/10.1038/354056a0.
[6] Cheng H, Zhang H, Zhao Y, Feng Y, Rui XF, Munroe P, et al. Doping effect of nano-diamond on superconductivity and flux pinning in MgB_2. Supercond Sci Technol 2003;16(10). https://doi.org/10.1088/0953-2048/16/10/310.
[7] Soltanian S, Horvat J, Wang XL, Munroe P, Dou SX. Effect of nano-carbon particle doping on the flux pinning properties of MgB_2 superconductor. Physica C 2003;390(3):185–90. https://doi.org/10.1016/S0921-4534(03)00960-2.
[8] Ueda S, Yamamoto A, Shimoyama J, Horii S. Enhanced critical current properties observed in Na_2CO_3-doped MgB_2. Supercond Sci Technol 2004;17(7):926. https://doi.org/10.1088/0953-2048/17/7/017.
[9] Ye SJ, Matsumoto A, Zhang YC, Kumakura H. Strong enhancement of high-field critical current properties and irreversibility field of MgB_2 superconducting wires by coronene active carbon source addition via the new B powder carbon-coating method. In: Superconductor Science and Technology; 2014. https://doi.org/10.1088/0953-2048/27/8/085012.
[10] Kim JH, Yeoh WK, Xu X, Dou SX, Munroe P, Rindfleisch M, Tomsic M. Superconductivity of MgB2 with embedded multiwall carbon nanotube. Physica C Supercond 2006;449(2):133–8. https://doi.org/10.1016/j.physc.2006.08.003.
[11] Dou SX, Yeoh WK, Horvat J, Ionescu M. Effect of carbon nanotube doping on critical current density of MgB_2 superconductor. Appl Phys Lett 2003;83:4996. https://doi.org/10.1063/1.1634378.
[12] Chandra S, Rajiv G, Malik SK, Srivastava ON. Improved critical current density of MgB_2– carbon nanotubes (CNTs) composite. J Nanosci Nanotechnol 2007;6:1804–9. https://doi.org/10.1166/jnn.2007.720.
[13] Yeoh WK, Kim JH, Horvat JS, Dou X, Munroe P. Improving flux pinning of MgB2 by carbon nanotube doping and ultrasonication. Supercond Sci Technol 2006;19(2). https://doi.org/10.1088/0953-2048/19/2/L01.
[14] Yeoh WK, Horvat J, Dou SX, Munroe P. Effect of carbon nanotube size on superconductivity properties of MgB_2. Ieee Trans Appl Supercond 2005;15(2):3284–7. https://doi.org/10.1109/TASC.2005.848853.
[15] Patel D, Maeda M, Choi S, Seong JK, Shahabuddin M, Parakandy JM, et al. Multiwalled carbon nanotube-derived superior electrical, mechanical and thermal properties in MgB_2 wires. Scr Mater 2014;88(13–16). https://doi.org/10.1016/j.scriptamat.2014.06.010.
[16] Yeoh WK, Horvat J, Kim JH, Xu X, Dou SX. Effect of carbon substitution on the superconducting properties of MgB_2 doped with multi-walled carbon nanotubes and nano carbon. Ieee Trans Appl Supercond 2007;17(2). https://doi.org/10.1109/TASC.2007.899418.
[17] Wei J, Li Y, Xua C, Wei B, Wu D. Structure and superconductivity of MgB_2–carbon nanotube composites. Mater Chem Phys 2003;78:785–90. https://doi.org/10.1016/S0254-0584(02)00391-7.
[18] Gong J, Wu J, Guan Z. Examination of the indentation size effect in low-load vickers hardness testing of ceramics. J Eur Ceram Soc 1999;19(15):2625–30. https://doi.org/10.1016/S0955-2219(99)00043-6.
[19] Gong J, Zhao Z, Guan Z, Miao H. Load-dependence of knoop hardness of Al_2O_3-TiC composites. J Eur Ceram Soc 2000;20(12):1895–900. https://doi.org/10.1016/S0955-2219(00)00093-5.
[20] Gong J, Miao H, Zhao Z, Guan Z. Load-dependence of the measured hardness of Ti(C, N)-based cermets. Mater Sci Eng A 2001;303(1):179–86. https://doi.org/10.1016/S0921-5093(00)01845-1.
[21] Bekteş M, Uzun O, Aktürk S, Ekinci AE, Uçar N. Vickers microhardness studies of Fe-Mn binary alloys. Chinese J Phys Lett 2004;42(6):733–9. https://doi.org/10.6122/CJP.
[22] Şahin O, Uzun O, Kölemen U, Düzgün B, Uçar N. Indentation size effect and microhardness study of β-Sn single crystals. Chinese J Phys Lett 2005;22(12):3137–40. https://doi.org/10.1088/0256-307X/22/12/043.

[23] Uzun O, Karaaslan T, Göğebakan M, Keskin M. Hardness and microstructural characteristics of rapidly solidified Al–8–16 wt.%Si alloys. J Alloy Compd 2004; 376(1–2):149–57. https://doi.org/10.1016/j.jallcom.2004.01.017.
[24] Uzun O, Kölemen U, Çelebi S, Güçlü N. Modulus and hardness evaluation of polycrystalline superconductors by dynamic microindentation technique. J Eur Ceram. Soc 2005;25(6):969–77. https://doi.org/10.1016/j.jeurceramsoc.2004.03.031.
[25] M. Bekteş. Fe-Mn alaşımlarının microhardness ölçümleri, Süleyman Demirel University, Institute of Science, 2004 Isparta, Master's Thesis.
[26] Quinn JB, Quinn VD. Indentation brittleness of ceramics: a fresh approach. J Mater Sci 1997;32(16):4331–46. https://doi.org/10.1023/A:1018671823059.
[27] Li H, Bradt RC. The effect of ındentation-ınduced cracking on the apparent microhardness. J Mater Sci 1996;31(4):1065–70. https://doi.org/10.1007/BF00352908.
[28] Upit GP, Varchenya SA. Microhardness of alkali halide crystals. Phys. Status Solidi A 1966;17(2):831–5. https://doi.org/10.1002/pssb.19660170242.
[29] Bull SJ, Page TF, Yoffe PEH. An explanation of the indentation size effect in ceramics. Mag Lett 1989;59:281–8. https://doi.org/10.1080/09500838908206356.
[30] Shafi PM, Bose AC. Impact of crystalline defects and size on X-ray line broadening: a phenomenological approach for tetragonal SnO_2 nanocrystals. AIP Adv 2015;5 (5):057137. https://doi.org/10.1063/1.4921452.
[31] Suryanarayana C, Norton MG. X-Ray diffraction a practical approach. New York: Plenum Publishing Corporation; 1998. p. 212 (1. Press).
[32] Öztürk Ö, Gökçen T, Çavdar S, Koralay H, Tascı AT. A study on nucleation, crystallization kinetics, microstructure and mechanical properties of Ru–Bi partial substituted BSCCO glass ceramics. J Therm Anal Calorim 2016;123:1073–82. https://doi.org/10.1007/s10973-015-5028-8.
[33] Çavdar S, Kol N, Koralay H, Öztürk Ö, Aşıkuzun E, Tascı AT. Structural, electrical and mechanical properties of selenium doped thallium based high-temperature superconductors. Cryogenics 2015;73:1–7. https://doi.org/10.1016/j.cryogenics.2015.10.019.
[34] Elmustafa AA, Stone DS. Nanoindentation and the indentation size effect: kinetics of deformation and strain gradient plasticity. J Mech Phys Solids 2003;51(2): 357–81. https://doi.org/10.1016/S0022-5096(02)00033-9.
[35] Kölemen U. Analysis of ISE in microhardness measurements of bulk MgB_2 superconductors using different models. J Alloy Compd 2006;425:429–35. https://doi.org/10.1016/j.jallcom.2006.01.075.
[36] Koralay H, Arslan A, Çavdar Ş, Öztürk Ö, Aşıkuzun E, Günen A, et al. Structural and mechanical characterization of $Bi_{1.75}Pb_{0.25}Sr_2Ca_2Cu_{3-x}Sn_xO_{10+y}$ superconductor ceramics using Vickers microhardness test. J Mater Sci Mater Electr 2013;24(11): 4270–8. https://doi.org/10.1007/s10854-013-1396-7.
[37] Tosun M, Ataoğlu S, Arda L, Öztürk Ö, Aşıkuzun E, Akcan D, et al. Structural and mechanical properties of ZnMgO nanoparticles. Mater Sci Eng A 2014;590:416–22. https://doi.org/10.1016/j.msea.2013.10.024.